Finite element modelling of bending of CFRP laminates: multiple delaminations

H. ULLAH[1]*, A.R. HARLAND[1], T. LUCAS[2], D. PRICE[2], V.V. SILBERSCHMIDT[1]

[1] Wolfson School of Mechanical and Manufacturing Engineering, Loughborough University, Leicester-shire, LE11 3TU, UK; [2] Adidas AG, Herzogenaruch, GERMANY

ABSTRACT

Carbon fibre-reinforced polymer (CFRP) composites are widely used in aerospace, automotive and construction structures thanks to their high specific strength and stiffness. They can also be used in various products in sports industry. Such products can be exposed to different in-service conditions such as large bending deformation and multiple impacts. In contrast to more traditional homogeneous structural materials like metals and alloys, composites demonstrate multiple modes of damage and fracture due to their heterogeneity and microstructure. Damage evolution affects both their in-service properties and performance that can deteriorate with time.

These failure modes need adequate means of analysis and investigation, the major approaches being experimental characterisation and numerical simulations. This research deals with a deformation behaviour and damage in composite laminates due to quasi-static bending. Experimental tests are carried out to characterise the behaviour of a woven CFRP material under large-deflection bending. Two-dimensional finite element (FE) models are implemented in the commercial code Abaqus/Explicit. A series of simulations is performed to study the deformation behaviour and damage in CFRP for cases of high-deflection bending. Single and multiple layers of bilinear cohesive zone elements are employed to model the onset and progression of inter-ply delamination process. Numerical simulations show that damage initiation and growth are sensitive to a mesh size of cohesive zone elements. Top and bottom layers of a laminate experience mode-I failure whereas central layers exhibit a mode-II failure behaviour. The obtained results of simulations are in agreement with experimental data.

Keywords: Composites, Large-deflection bending, Finite element models, Cohesive-zone element, Delamination

* Corresponding author: Ashby Road, Loughborough, Leics., LE11 3TU, UK.

Phone: +44-1509-227534. Fax: +44-1509-227502. E-mail: H.Ullah@lboro.ac.uk

1. Introduction

Composite materials, especially carbon fibre reinforced plastics (CFRP), have found many applications in aerospace, automotive, medical and construction components and structures due to their better specific strength and stiffness. Woven-fabric composite laminates offer a number of attractive properties compared to their unidirectional-tape counterparts such as lower production costs, better drapability, good resistance to fracture and transverse rupture due to weaving resistance, and high impact strength [1, 2]. These properties have attracted the sports industry to incorporate woven CFRP laminates in the design of sporting goods. Such products could be subjected to large-deflection bending and multiple impacts in service conditions. These quasi-static and dynamic loads generate high local stresses and strains leading to complex damage modes due to heterogeneity and anisotropy of composite laminates. In a bending scenario, a laminate experiences transverse shear and normal stresses resulting in the interlaminar delamination damage, because of their low through-thickness strength and stiffness [3]. Damage evolution results in significant reduction of in-service mechanical properties and leads to a loss of structural integrity of the composite sports products with time.

Computational damage modelling of delamination requires the capability to model initiation and progression of damage during analysis. Delamination initiation in composite laminates is usually assessed by strength-based criteria; for instance, the maximum nominal stress and quadratic strength criteria are used successfully for this purpose. Several techniques based on fracture-mechanics approach are employed in the finite element method (FEM) to simulate a delamination growth such as the J-integral, the virtual crack extension technique and the virtual crack closure technique (VCCT) [4]. Fracture-mechanics analysis is limited in this respect since it neglects material's nonlinearity and requires the position of delamination crack to be known in advance [5]. Further, typically, a fine mesh around the crack front is

required, which makes the analysis of three-dimensional composite structures more computationally expensive. Therefore, numerical prediction of the effects of interlaminar damage on the behaviour of composite laminate requires a finite-element scheme that is capable to model strength as well as toughness of the inter-ply layers.

A reliable and promising approach to overcome the above issues and model the material as well as geometric nonlinearities is to employ cohesive elements at the interface between the composite laminas. Cohesive-zone elements are based on the model proposed by Dugdale [6], who introduced the concept that stresses in the material are limited by the yield stress and that a thin plastic zone is generated in front of the crack. Barenblatt [7] introduced an idea of cohesive forces on a molecular scale in order to solve the problem of equilibrium in elastic bodies consisting of cracks. Needleman [8] was one of the first to use polynomial and exponential types of cohesive-zone models to describe the process of void nucleation from initial debonding to complete decohesion in metal matrices. Cohesive-zone elements are able to predict both the onset and growth of delamination combining the strength- and fracture-based approaches in a single finite-element model without preliminary knowledge of a crack's location and propagation direction [9].

Cohesive-zone damage models define relationships between tractions and displacements at an interface, where a crack may occur. Damage initiation in this case is related to interfacial strength, i.e., the maximum traction on the traction–displacement jump relation, at which reduction of material's stiffness starts. The stiffness degradation continues until the interface elements attain zero stiffness, corresponding to complete separation of adjacent layers. After this the interface elements act only as a contact region without transferring loads from them. The work required to reduce the material's stiffness to zero is equal to the fracture toughness, i.e. the area under the traction–displacement curve [10].

In case of modelling composite delamination, cohesive-zone schemes offer a number of advantages over other modelling approaches, as they have the capacity to model both initiation and growth of damage in the same analysis, incorporating concepts of both the damage-mechanics and fracture-mechanics theories. However, application of cohesive-zone elements to model progressive delamination in composite structures poses numerical difficulties related to the proper definition of

stiffness of the interface layer, the requirement of highly refined finite-element meshes, and convergence difficulties associated with a softening behaviour of the interface material [11]. Moreover, an ideal cohesive model should be able to model stable as well as unstable crack propagations and the transitions between the propagation regimes [12].

Quasi-static and dynamic loading of composite laminates result in complex damage mechanisms, in which multiple delaminations and interfacial fractures are dominant ones. Damage initiation and growth in composite structures subjected to bending loads have been studied by numerous researchers, using various FE models [13-16]. However, these models are usually developed in the context of a static or steady-state crack propagation using implicit FE tools. Therefore, a further research work is needed to develop reliable FE models capable of simulating the damage progression behaviour of laminated composites under large-deflection bending loads resulting in more rational and optimised designs. However, these high-fidelity simulations of discrete damage behaviour of composite laminates should be based on experimental studies of damage mechanisms to adequately represent their in-service performance. To overcome these problems, this paper presents an efficient numerical simulation of interlaminar damage propagation in woven CFRP laminates under transverse loading, using a cohesive-zone element method.

2. Experimental tests

Reliable and accurate numerical modelling of discrete damage behaviour of composite laminates should be based on experimental characterisation of damage mechanisms corresponding to real-world loading scenarios. Experimental tests were conducted to obtain material properties and validate numerical models. This objective was achieved by testing two types $[0°]_6$ and $[90°]_6$ CFRP specimens under three-point bending conditions. These specimens were fabricated from carbon-fibre fabric woven in 2/2 twill reinforcement in thermoplastic polyurethanes (TPU) polymer with a fibre volume fraction of 45 %; the fabric has the same number of yarns in the warp and weft directions. Water-jet cutting was used to prepare rectangular specimens of 80 mm length, 25 mm width and 1.5 mm thickness, each laminate having six plies of 0.25 mm thickness. This cutting technique resulted in high surface finish of the samples without causing any damage in the fibres and matrix. Flexural

tests were carried out at indenter speed of 100 mm/min, equivalent to a strain rate of 0.042/s, using the Instron 5569 machine in accordance with the ISO 178 standard. Five samples per orientation were tested under large-deflection bending until their ultimate fracture.

Both 0° and 90° CFRP samples exhibited a brittle failure response in flexure as shown in Figs.1 and 2. The tests resulted in the same flexural modulus of 44.7 GPa and ultimate flexural strengths of 833 MPa and 824 MPa for 0° and 90°, respectively. This similarity is due to the symmetry of fibres in both warp and weft directions in both types of samples. Stiffness degradation due to internal cracks and delamination occurs in 0° sample at about 80% of the ultimate load, where as 90° sample show no stiffness reduction before ultimate fracture. Although the samples undergo cracking and interlaminar damage before the structure loses its load carrying capacity, the development of such inter-ply delamination is not reflected in the stress-strain diagram, i.e. the effect of these usually hidden and barely visible damage mechanisms is small. A typical failure pattern of 0° CFRP specimen in Fig. 2 shows that damage is distributed through the width at the centre of laminate. The character of ultimate fracture demonstrates that fibres of the specimen's top surface, which are in compression, remain intact (Fig. 2a), whereas fibres of the bottom surface, experiencing tension, are fractured (Fig. 2b). The elastic flexural moduli such as E_{11} and E_{22} were calculated from the mechanical tests of 0° and 90°, respectively, and are listed in Table 1. Rest of the elastic properties in Table 1 were taken from [12], where a similar CFRP textile laminate was studied.

3. Finite-element modelling

Failure prediction of fibre-reinforced composite laminates is complicated by their heterogeneous nature, which gives rise to various types of multiple cracks, interacting strongly as failure progresses. These damage mechanisms may cause significant redistribution of stresses and thus affect the load level, at which final structural failure occurs. Design and certification of most composite structures are based on empirical approaches because of the difficulty of complete damage-process prediction, with relatively little use of simulations. Therefore, there is a need for models, which are capable of simulating the entire damage process from its initiation through evolution to complete composite structure failure. Analytical models

are impractical and, probably, unable to model this complex damage process, initiating from matrix cracking, evolving in delamination and fibre breakage to composite structural ultimate failure. The most promising and suitable tool is a computational approach based on the finite element method (FEM). This approach unlocks a full potential of composites resulting in more rational and optimised design of composite laminated structures. However, the development of proper numerical model representing the physics of damage mechanisms is a challenging task [17].

Reliable and accurate simulations of discrete damage behaviour of composite laminates require guidance from experimental and theoretical studies of damage mechanisms. Understanding a sequence of different damage modes in ply-scale damage and physical parameters in material's constitutive laws that determine which mode will dominate is a challenge of respective simulations. According to Cox and Yang [18], the difficulty in composite damage modelling is linked not only to insufficient computational power. A more serious challenge is to categorise and characterise many possible mechanisms of damage and represent them in a model in a realistic and physical way. Similarly, understanding the origin of numerical instabilities that often occur in simulations of heterogeneous materials poses another challenge. It is critical to know whether these instabilities are due to numerical approximations or rather they reflect physically unstable damage propagation, such as the dynamic crack propagation that is often observed in experiments. Modelling of cracking sequences and potential instabilities successfully in a computationally cost-effective way is of key interest to developing tools for use as virtual tests [19]. In this study, various approaches are implemented in finite-element models to characterise the onset and progression of damage for analysis of composite structures. The studies involve monitoring of a particular type of parameter such as stiffness degradation for prediction and monitoring of damage growth.

3.1. Modelling strategy

Our finite element models are developed in the commercial FE package ABAQUS/Explicit to investigate large-deflection bending of tested composite laminates and the resulting interlaminar damage. An explicit dynamic analysis approach is typically adopted to model large deflection, material nonlinearity and contact in high-velocity transients but it can be also employed effectively in modelling dynamic phenomena with severe discontinuities in the structural response, as occurs

in unstable crack propagation. However, an explicit time integration scheme requires a small time increment size Δt that depends on the highest natural frequency ω_{max} of the structure and is given as [20]

$$\Delta t \leq \frac{2}{\omega_{max}}, \qquad (1)$$

Therefore, first, an eigenvalue analysis of the undamaged laminate was carried out to determine the structure's natural frequency in order to define the first estimate of time increment for stable solution. However, in nonlinear problems, the highest frequency of the model will continually change, which consequently changes the stability limit. Thus, the time increment value is reduced to obtain a converged solution with activating automatic time inceremention. Since the analysis is quasi-static, the computational time of the simulation is directly proportional to the number of time increments required and size of the FE mesh. The number of increments required is $n = T/\Delta t$; depends upon Δt, if the time period T of the simulated event remains constant. Hence, in a two-dimensional analysis, refining the mesh by a factor of two in each direction will increase the run time in the explicit procedure by a factor of eight (four times as many elements and half the original time increment magnitude). However, this magnitude should not be too large to lose the accuracy and convergence of nonlinear large-deformation simulation involving damage.

Three FE models A, B and C as shown in Fig. 3 are developed representing the bending tests on an 80 mm long, 25 mm wide and 1.5 mm thick CFRP laminate. Model A contains a single cohesive layer above the beam's neutral axis (NA), model B has two interface layers - one above NA and second coinciding with it, whereas model C has three cohesive layers - above, on and below the NA to simulate multiple delamination scenarios. The cohesive layer above the NA is referred as top cohesive layer (TCL), the cohesive layer on the NA is referred to as mid cohesive layer (MCL) and the one below the NA is referred to as bottom cohesive layer (BCL). Theoretically, many interlaminar layers may be included in the model since the location of damage initiation is not *a priori* known. However, in such a case, the modelling effort, the complications due to the calibration of the penalty stiffness, and the computational times may increase, and the solution convergence becomes

rather complicated. Further, the number of cohesive layers in FE models should be such that the structure may be able to carry the applied load without losing its global stiffness before the damage starts in the actual laminate. That is why numerical predictions of composite damage should be based on experimental evidence. To model the actual global stiffness of the structure, the maximum of three cohesive layers are introduced in model C. Further, in three - point bending, the layers above and below the NA experience compression and tension respectively due to normal bending stress, whereas the mid layers are subjected to shear. Therefore, the cohesive layers at these locations are defined to simulate both the single and mixed-mode fracture mechanisms.

The laminate has a considerable length in z-direction, thus, generalised plane strain conditions are assumed. Two-dimensional FE models based on plane-strain elements with linear shape functions are developed to represent in-plane bending behaviour in a computationally cost effective manner. Composite laminas are meshed with plane-strain reduced integration and hourglass control CPE4R elements capable of eliminating the shear locking in bending problems, using the structured meshing technique. Interlaminar cohesive layers are meshed with two-dimensional COH2D4 elements using sweep mesh control. The interface region is discretized with a single layer of infinitesimally small thickness cohesive elements having shared nodes with ply elements. The beam's meshes include two elements per lamina along the thickness to reproduce the stacking sequence of the laminate, and capture the normal and shear stress distributions through thickness and control the hourglassing. Indenter load application is represented by a circular arc at the centre of the beam that is also laterally supported by two other circular arcs, which are set at a distance of 40 mm along the beam's axis to replicate experimental tests. All three circular arcs have been considered to be rigid with a diameter of 5 mm. Surface-to-surface explicit contact is defined between the rigid arcs and the laminate top and bottom surfaces. The overhanging length of the beam L (edge) in Fig. 3 is 20 mm where the distance between the supports and indenter L (mid) is also kept at 20 mm. All composite laminas are assigned elastic properties shown in Table 1. Interlaminar strengths and fracture toughness are indentified by numerical analyses. Normal σ_{I0} and shear σ_{II0} strengths are calibrated with the FE analysis of the undamaged beam under the same boundary conditions. In the FE analysis, the

interlaminar shear stress is recorded as the respective strength of the composite laminate at the moment of failure measured in experimental tests of the CFRP laminate. This is based on the approach for numerical determination of interlaminar shear strength of composite laminates under bending, developed in [21, 22] and employed in [23]. Similarly, normal stress at the ultimate load is taken as the normal strength of the laminate. The fracture toughness in mode I G_{Ic} and mode II G_{IIc} are indentified by numerical analyses based on the approach adopted in [12] for numerical analysis of beams. The fracture toughness values are calibrated based on numerical optimisation so that the corresponding FE model was capable to represent damage in the bending test of the laminate.

3.2. Multiple delamination modelling using cohesive- zone elements

Interlaminar damage in the resin-rich region between plies of a laminate is usually an invisible threat to structural integrity of composites. Computational models with the capability to predict the initiation and progression of delaminations can reduce the number of costly experimental tests and can lead to improved designs. Cohesive-zone elements (CZE) have the ability to capture the onset and propagation of delamination [9, 10]. Cohesive elements can be defined at various locations in FE models, and the analysis will determine which one, or what combination of potential delaminations will develop. The elements can also be placed between every ply of a laminate, although it is not necessary to place them at interfaces between plies of the same orientations where delaminations occur rarely [24]. The cohesive behaviour assumes that failure of the elements is characterized by progressive degradation of the material stiffness, which is driven by a damage process.

3.2.1 Delamination initiation and progression

Delamination failures in composite laminates initiate and propagate under the combined influence of normal and shear stresses. The nonlinear constitutive behaviour of the CZE under mode-I and mode-II fracture is defined by a bilinear traction–separation law. Damage initiation is related to the maximum traction on the traction – displacement curve, followed by a linear softening phase that simulates the progressive decohesion of the interface with increasing damage. The interface is

completely fractured when cohesive tractions vanish at the end of the softening phase. The maximum nominal stress criterion is used for damage initiation. Delamination propagation is usually predicted by criteria established in terms of the energy release rates and fracture toughness under mixed-mode loading. This study is based on the power law criterion proposed by Reeder [25]

$$\left(\frac{G_I}{G_{IC}}\right)^n + \left(\frac{G_{II}}{G_{IIC}}\right)^n + \left(\frac{G_{III}}{G_{IIIC}}\right)^n = 1 \ , \qquad (2)$$

where G_I, G_{II}, and G_{III} are the energy release rates in modes I, II, and III, respectively, and G_{IC}, G_{IIC}, and G_{IIIC} are the corresponding critical energy release rates.

3.2.2 Discretization and mesh convergence

Presence of CZEs in FE model defines the crack propagation path. The extent of crack growth along the prescribed path defined by CZEs depends on the size of these elements as the cohesive-zone model is a local approach. Thus, the application of CZE requires a fine spatial discretization at the cohesive zone to capture the damage growth properly. However, such refinement may be prohibitive since it needs a significant increase in computational efforts [26]. An optimum number of elements are required in the cohesive zone to obtain accurate numerical results. In case of a coarse mesh used for a cohesive-zone, the distributions of tractions ahead of the crack tip are not represented accurately. Different models have been proposed in the literature to estimate the length of the cohesive zone, l_{cz} [6, 7, 10]. This length is defined as the distance from the crack tip to the point where the final failure point is reached. The number of elements N_e in a cohesive zone according to [10], is given by

$$N_e = \frac{l_{cz}}{l_e} \ , \qquad (3)$$

where l_e is the mesh size in the direction of crack propagation. However, the minimum number of CZEs is not well established. Further, all these models are based on pre-existing and pre-defined cracks in the laminate such as in simulating double cantilever beam (DCB) and mixed-mode bending (MMB) etc. tests. No accurate model is available to determine the cohesive element size for the FE model of the undamaged state before load application.

In this paper, the model proposed by Turon *et al.* [10] is used in the numerical analysis to obtain an initial estimate of the cohesive zone length and the interface element size defined by equation (3). Before performing further simulations, a mesh convergence study was performed on model A with a single cohesive layer. Four FE models are developed with different element lengths ranging from 0.05 mm to 0.4 mm. The thickness of all interface elements is 2 μm; the total thickness of the laminate remains unchanged. The laminate is meshed with fine structured elements of aspect ratio 1 to avoid premature solution termination because of elements distortion due to geometric as well as material nonlinearities. The performed mesh study with different element lengths is summarized in Fig.4. The results indicate that by decreasing the element length, the damage zone along the laminate length increases and solution convergence is achieved. Mesh 3 of 0.1 mm element length is selected for computationally effective simulations of single and multiple deleminations in numerical models A, B and C. A similar behaviour of CZE is also shown in [27], indicating that as long as the interface element size is taken less than 1 mm, numerical results are in agreement with experiments and a better solution convergence is achieved.

3.2.3 Stiffness of cohesive-zone elements

Interface elements act as load-transfer connections between the continuum elements before the onset of delamination. Since cohesive elements represent zero- or infinitesimal-thickness interfaces, high stiffness is required to model the connections. Therefore, the interface stiffness should be large enough to avoid relative displacements between the connected ply elements but also not too large to cause numerical problems such as spurious oscillations in interfacial traction of the cohesive element [11, 12, 27]. This stiffness is usually calibrated by numerical

simulations as it cannot be measured directly through the experiments. Several authors have proposed different methods to calibrate the cohesive element stiffness. Camanho *et al.* [9] obtained accurate results by using 10^6 N/mm^3 for graphite-epoxy specimens. Turon *et al.* [11] demonstrated that elastic properties of the composite would not be affected if the interface stiffness is defined as

$$K = \frac{\alpha E_{33}}{t_{\mathrm{p}}} \ , \qquad (4)$$

where E_{33} is the material's through-thickness stiffness of the material, t_{p} is the thickness of ply connected by the cohesive element, and α, is a non dimensional parameter, which should be greater than 50 for accurate simulation of various problems. Based on equation (4), value of interface stiffness, 3x10^6 N/mm^3 was used as a first estimate in this study. The stiffness was increased gradually until convergence was achieved at 8 x 10^6 N/mm^3.

3.3 Boundary conditions and solution

Simply supported boundary conditions are applied at the reference points of the rigid supports below the laminate representing the test fixture. A displacement-controlled load is applied at the centre rigid arc representing the indenter, which is in contact with the top ply of the laminate, for better convergence of the solution. Boundary conditions are applied at rigid surfaces instead of constraining the ply nodes as the local stresses due to the constraints edge effects disperse over greater distances of the structure because of the composite's anisotropy. As shown by Horgan *et al.* [28] for anisotropic composite materials, the application of St. Venant's principle for plane elasticity problems involving anisotropic materials is not justified in general. The displacement is applied gradually to obtain a stable and converged solution at each equilibrium iteration for a particular time step. The model is solved using the explicit solver capable of overcoming convergence difficulties due to the material softening behaviour and stiffness degradation after the onset of damage. Quasi-static analysis is carried out for 0.1 second with large-deflection effects by applying the load in small time increments of 10^{-7} seconds to capture the damage process in the CZE. The

final FE model C contained a total of 11,715 elements which took 4 hours on a dual core machine with two 2.7 GHz processors each. The computational cost is a direct consequence of a fine mesh coupled with the highly nonlinear behaviour of interface damage elements.

4. Results and discussion

Numerical results of our simulations of the large-deflection bending behaviour of CFRP laminates and comparison with experimental tests are presented in this section. The experimental tests resulted in the same flexural behaviour due to the symmetry of fibres in both warp and weft directions in both types of 0° and 90° samples. Damage initiation and progression along a single cohesive layer above the neutral plane of the beam in FE model A is shown in Fig.5. Damage is represented by normalised length (L_d/L) of the cohesive layer along the beam axis against the normalised displacement loading (δ/δ_f), where δ_f is the displacement at the ultimate failure of the test specimen. Figure 5 shows that the overhang region L (edge) outside the beam supports is more vulnerable to damage than the inside region L (mid). The damage in the overhang initiates at 20% of the total load lower than in the mid-region, which is at about 50%. The delamination process in this model is of mode-I type triggered by normal stresses above the neutral plane. Similarly, delamination progresses more in the overhang than the mid-region before the ultimate failure. The initiation and progression behaviours of multiple delaminations in model B are demonstrated inFig.6. Here too, delamination initiates faster in the overhang regions of the top and mid cohesive layers than in the mid-region. The overhang exhibits mode-I fracture whereas the mid-region is in mode-II state. However, the delamination grows more rapidly in the MCL than TCL in the beam's mid-region until the MCL is completely damaged. This behaviour is more exaggerated in the results of multiple delmainations in model C shown in Figs. 7 and 8. Figure 7 demonstrates that although delamintion initiates earlier in the beam's edges, it grows more in the mid-section. The MCL is more damaged due to mode-II shear fracture as shown in Fig. 8. The reason for this is that the maximum through-thickness shear stresses generally occur in the mid-section of the laminate and drive the mode-II delamination process. Further, the mid-region exhibits mode-II delamination as the shear stresses outside the beam's supports diminish as shown

in Fig. 10. Variation of flexural stress σ_{xx} along the beam thickness in model C is shown in Fig. 9. Figure 10 displays the contour of interlaminar shear stress τ_{xy} in model C under three-point bending. Interlaminar shear stress (ILSS) exists between the supports as shown in Fig. 10, and its value diminishes outside the beam supports, as the shear force vanishes there. The letters L, M and S in Fig. 10 indicate the locations of loading, mid-span between loading and support, and support, respectively, for investigation of the ILSS profile and distribution through the thickness. Contour plots of the ILSS at these locations are presented in Fig. 11. The ILSS distribution through the thickness computed at the nearest Gauss points to points L, M and S in Fig. 10 are illustrated in Fig. 12. The ILSS concentrations in the vicinity of the loading point and the support rollers (points L and S) are very high but they rapidly decrease to values below the failure threshold at approximately 1/10 of the thickness for the CFRP laminate. Feraboli and Kedward [22] found this value as 1/12 of the thickness for carbon/epoxy composite laminates. It is evident from Figs. 11b and 12b, that at a distance away from the rollers, ILSS increases toward the middle i.e. the neutral axis of the beam. Transverse distribution of shear stresses is parabolic with a maximum value of 25 MPa at the central cohesive layer, which experienced mode-II fracture. A sharp increase of stress at the locations of cohesive layers i.e. crack tips, is apparent in Fig. 12, when the interlaminar failure occurs, as expected. Similarly, contour plots and distribution of normal stress σ_{yy} are presented in Figs. 13 and 14. Here, too, the loading and support points (L and S) experience high stress concentration as shown in Figs. 13, 14(a) and 14(c) but it decreases rapidly to lower values away from these locations. At the mid span between the loading point and support, normal stress is almost uniformly distributed , but varies at the cohesive layers as depicted in Figs 13 and 14 (b). In all the numerical models, delamination initiates at above 30% of the failure load and then propagates at a higher rate. Damage suddenly spreads after attainment of 70% of the failure load, especially in the middle section of the beam.

The developed numerical models are validated through comparison with experimental test data. The load-deflection behaviour obtained numerically for three different models and experimentally from three point bend tests of CFRP woven laminates is presented in Fig. 15. A good agreement is achieved between

experiments and numerical simulations indicating that the numerical models are capable to reproduce the failure of the laminate beams. It can be observed that the development of such interlaminar damage did not induce noticeable effects on the force vs. displacement curves till the stiffness degradation occur at points P, Q, R and T (Fig. 15). At these points the damage saturation occurs, followed by instantaneous loss of structure's load-carrying capability. However, such internal barely visible delamination damages can reduce the compressive strength of the composite and can result in buckling of the plies. Figure 15 shows that by increasing the number of cohesive layers in FE models, the structure loses its load-carrying capability earlier and ultimate failure occurs at a lower load level. Thus a reasonable number of cohesive layers should be defined in FE models to capture the real failure behaviour especially between the plies with different orientations, where the laminate is more susceptible to delamination initiation. Models A and B with one and two cohesive layers, respectively, reproduced the specimen's failure behaviour observed in tests. Further, all of the performed numerical simulations and the presented numerical–experimental comparison indicate that the response of composite laminates before the onset of delamination is adequately reproduced by the calibrated stiffness of the interface elements.

5. Conclusions

Damage in CFRP textile composites under large-deflection bending was studied using expeirmental tests and numerical simulations.The tests were carried out to characterise the behaviour of the woven CFRP material. Two-dimensional plane-strain finite-element models were implemented in the commercial code Abaqus using the explicit solver. A series of simulations was performed to study the onset and progression of inter-ply delamination process under mixed – mode large deflection bending by employing single and multiple layers of cohesive zone elements in the developed FE models.

The numerical results were quite close to the experimental ones and the numerical models have the capability to reproduce the failure mechanisms in composite laminates. The FE models provided more information than the experimental tests and helped to gain a better understanding of the damage initiation and evolution

processes in woven laminates. Numerical simulations showed that damage initiation and growth was sensitive to the mesh size of cohesive zone elements. The top and bottom layers of the laminate beam experienced mode-I failure whereas the central layers exhibit the mode-II failure behaviour. Application of the suggested numerical approach to the test cases proved the capability to model complex patterns of damage development in originally undamaged specimen. Damage that suddenly propagated and that subsequently led to an immediate loss of load-carrying capability was captured with the explicit dynamic approach. Overall, it should be noted that all of the modelled interlaminar layers in the finite-element schemes represented potential zones of damage nucleation and propagation. The results indicated the suitability of the developed numerical approach to study the onset and propagation of interlaminar damage. However, the calibration of numerical models based on interface layers proved to be highly mesh and stiffness sensitive and would certainly represent a critical issue in the application of the approach to real-world components and structures. The numerical results also revealed that in order to achieve a response closer to experimental tests, there must be some limitations on the values of cohesive elements' stiffness and size, which in turn influence the computational cost of simulations. It is also significant that all interface parameters must be calibrated and specified correctly in order to avoid long computational times, solution oscillations or even premature termination and obtain better convergence. Therefore, a complete investigation of the mesh's sensitivity of the results, identification of the interface stiffness and strength levels through experiments, and a comparison of the results, obtained by applying different constitutive laws, are required to develop more reliable and robust FE models.

References

[1] C. Hochard, J. Payan, C. Bordreuil, International Journal of Fatigue, 28 (2006) 1270-1276.

[2] G. Ernst, M. Vogler, C. Hühne, R. Rolfes, Composites Science and Technology, 70 (2010) 61-72.

[3] L. Iannucci, Computers & Structures, 84 (2006) 1029-1048.

[4] G. Wimmer, C. Schuecker, H.E. Pettermann, Composites Part B, 40 (2009) 158-165.

[5] G. Alfano, M.A. Crisfield, International Journal for Numerical Methods in Engineering, 50 (2001) 1701-1736.
[6] D.S. Dugdale, Journal of the Mechanics and Physics of Solids, 8 (1960) 100-104.
[7] G.I. Barenblatt, Advances in applied mechanics, 7 (1962) 104.
[8] A. Needleman, Journal of Applied Mechanics, 54 (1987) 525-531.
[9] P.P. Camanho, C.G. Davila, M.F. De Moura, Journal of Composite Materials, 37 (2003) 1415.
[10] A. Turon, P.P. Camanho, J. Costa, C.G. Dávila, Mechanics of Materials, 38 (2006) 1072-1089.
[11] A. Turon, C.G. Davila, P.P. Camanho, J. Costa, Engineering Fracture Mechanics, 74 (2007) 1665-1682.
[12] A. Airoldi, G. Sala, P. Bettini, Composites Science and Technology, doi:10.1016/j.compscitech.2009.10.011, 2009.
[13] M.G. Andrews, R. Massabò, A. Cavicchi, B.N. Cox, International Journal of Solids and Structures, 46 (2009) 1815-1833.
[14] F. Aymerich, F. Dore, P. Priolo, Composites Science and Technology, 69 (2009) 1699-1709.
[15] C. Santiuste, S. Sánchez-Sáez, E. Barbero, Composite Structures, 92 (2010) 2406-2414.
[16] P. Lonetti, Computational Materials Science, 48 (2010) 563-575.
[17] F.P. Van Der Meer, L.J. Sluys, Journal of Composite Materials, 43 (2009) 2131.
[18] B. Cox, Q. Yang, Science, 314 (2006) 1102-1107.
[19] Z. Zhou, X. Fang, B. Cox, Q. Yang, International Journal of Fracture, 165 (2010) 77-92.
[20] Hibbit, Karlsson, Sorensen, in, ABAQUS User's Manual, Version 6.10, Michigan, USA, 2010.
[21] J. Zhao, S.V. Hoa, X.R. Xiao, I. Hanna, Journal of Reinforced Plastics and Composites 18 (1999) 827.
[22] P. Feraboli, K.T. Kedward, Composites Part A, 34 (2003) 1265-1271.
[23] W.J. Na, in: Damage analysis of laminated composite beams under bending loads using the layer-wise theory, Texas A&M University, 2008.
[24] M.R. Wisnom, Composites Part A, 41 (2010) 795-805.
[25] J.R. Reeder, in: Technical Memorandum-1992-104210, NASA Langley Research Centre 1992.

[26] Z.R. Khokhar, I.A. Ashcroft, V.V. Silberschmidt, Computational Materials Science, 46 (2009) 607-613.

[27] P. Naghipour, J. Schneider, M. Bartsch, J. Hausmann, H. Voggenreiter, Engineering Fracture Mechanics, 76 (2009) 2821-2833.

[28] C.O. Horgan, J.G. Simmonds, Composites Engineering, 4 (1994) 279-286.

Table Captions

Table 1. Material properties of CFRP in FE model

Figure Captions

Fig. 1. Stress-strain diagram from flexural tests of twill 2/2 CFRP

Fig. 2. Fracture of twill 2/2 0^o CFRP specimen in three-point bending test: (a) top surface; (b**)** bottom surface

Fig. 3. FE models for damage simulation in three point bending

Fig. 4. Damage sensitivity to cohesive element size

Fig. 5. Damaged zone at the edge and middle of the beam - Model A

Fig. 6. Damaged zone at the edge and middle of the beam - Model B

Fig. 7. Damaged zone at the edge and middle of the beam - Model C

Fig. 8. Development of interlaminar damage in multiple cohesive layers under three-point bending

Fig. 9. Contour of bending stress σ_{xx} in Model C of three-point bending test

Fig. 10. Contour of interlaminar shear stress τ_{xy} in Model C of three-point bending test

Fig. 11. Contour of interlaminar shear stress τ_{xy} at load application point L (a); mid-span between loading and support, point M (b); and support point S (c); in Fig. 10

Fig. 12. Through-thickness distribution of Interlaminar shear stress at load application point L (a); mid-span between loading and support, point M (b); and support point S (c); in Fig. 10

Fig. 13. Contour of normal stress σ_{yy} at load application point L (a); mid-span between loading and support, point M (b); and support point S (c); in Fig. 10

Fig. 14. Through-thickness distribution of normal stress at load application point L (a); mid-span between loading and support, point M (b); and support point S(c); in Fig. 10

Fig. 15. Numerical and experimental load-displacement response of CFRP laminates under bending

Table(s)

Table 1. Material properties of CFRP considered in the FE model

Elastic property		Interlaminar strength	and toughness
$E_{11} = E_{22}$ (GPa)	44.7	σ_{I0} (MPa)	12
G_{12} (GPa)	4.4	σ_{II0} (MPa)	26
v_{12}	0.05	G_{Ic} (J/m^2)	800
E_{33} (GPa)	8.0	G_{IIc} (J/m^2)	1750
$G_{13} = G_{23}$ (GPa)	3.0		
$v_{13} = v_{23}$	0.3		

Figure(s)
Click here to download high resolution image

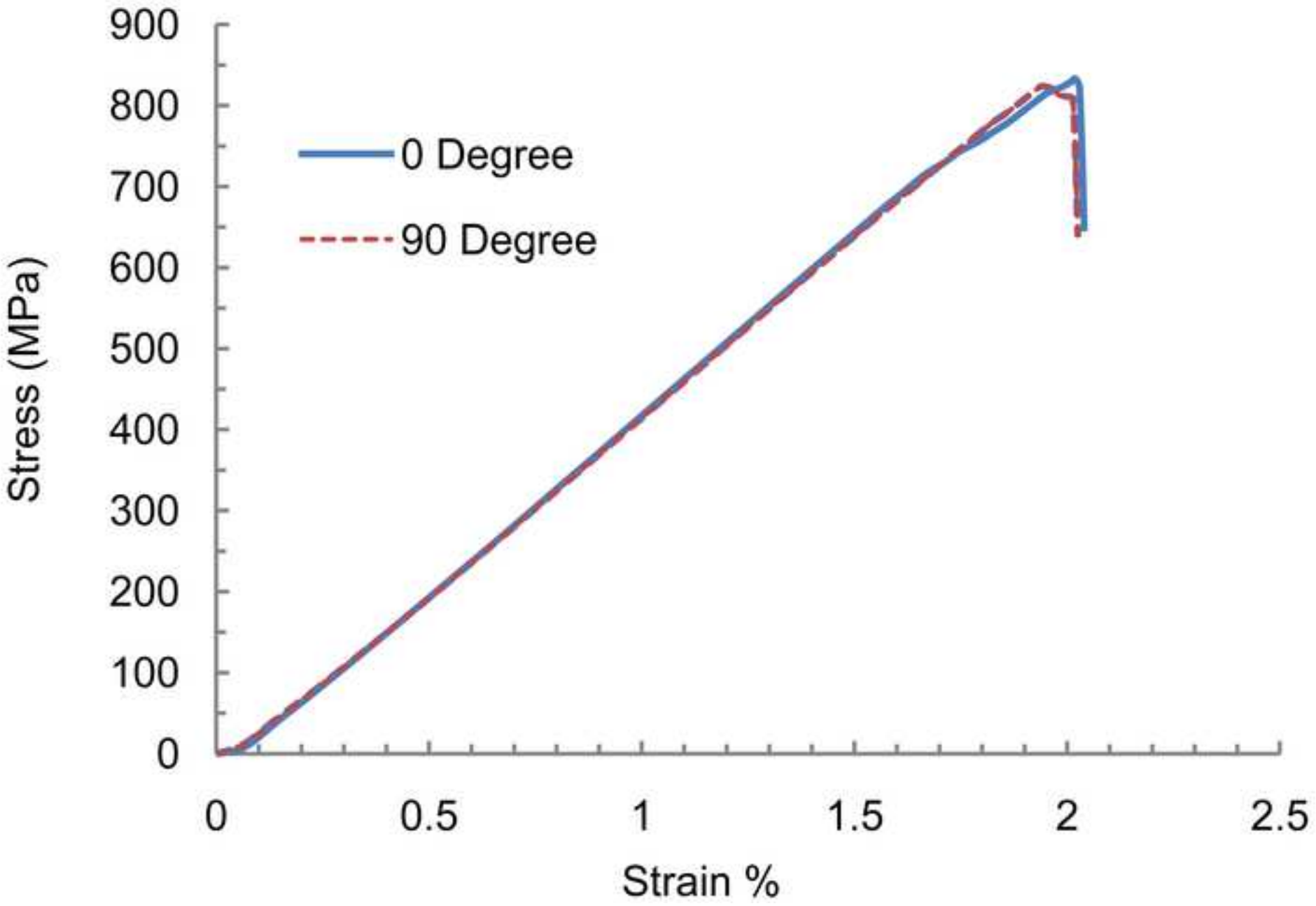

Figure(s)

Click here to download high resolution image

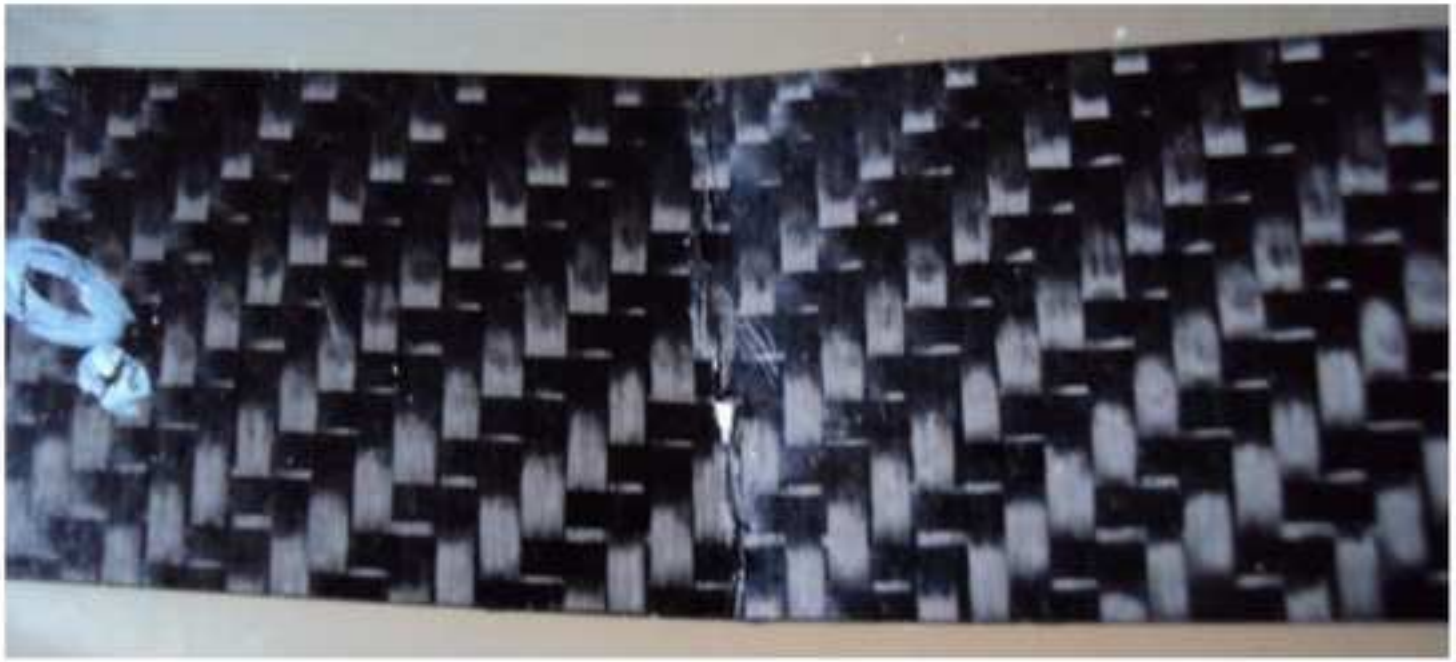

(a)

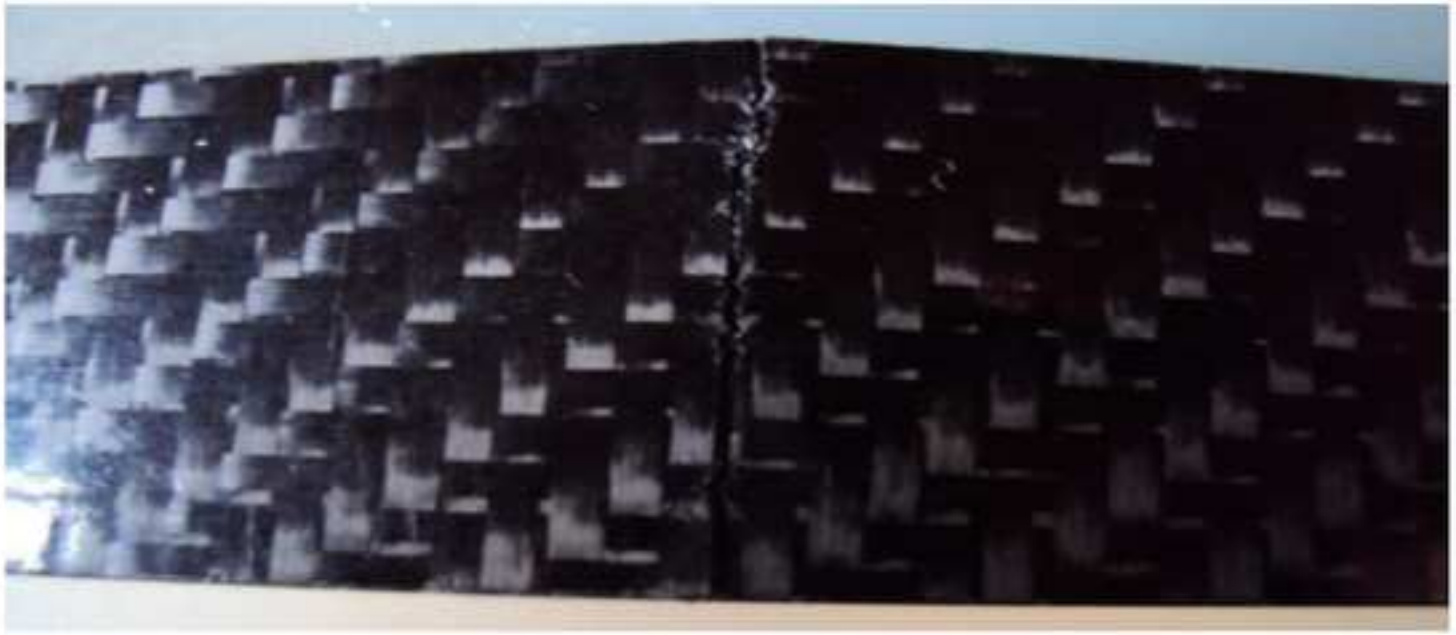

(b)

Figure(s)

Click here to download high resolution image

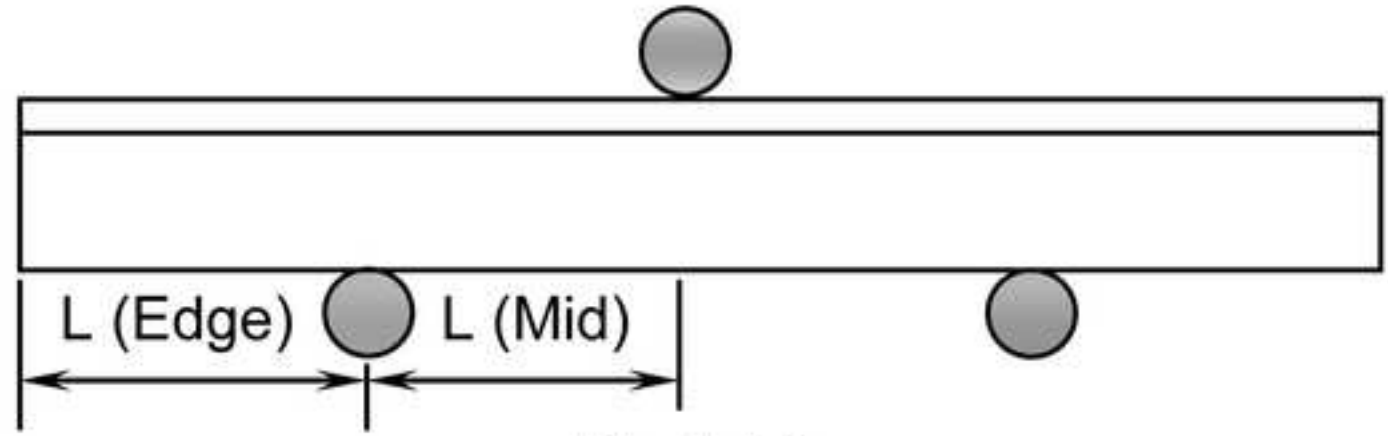

Model A

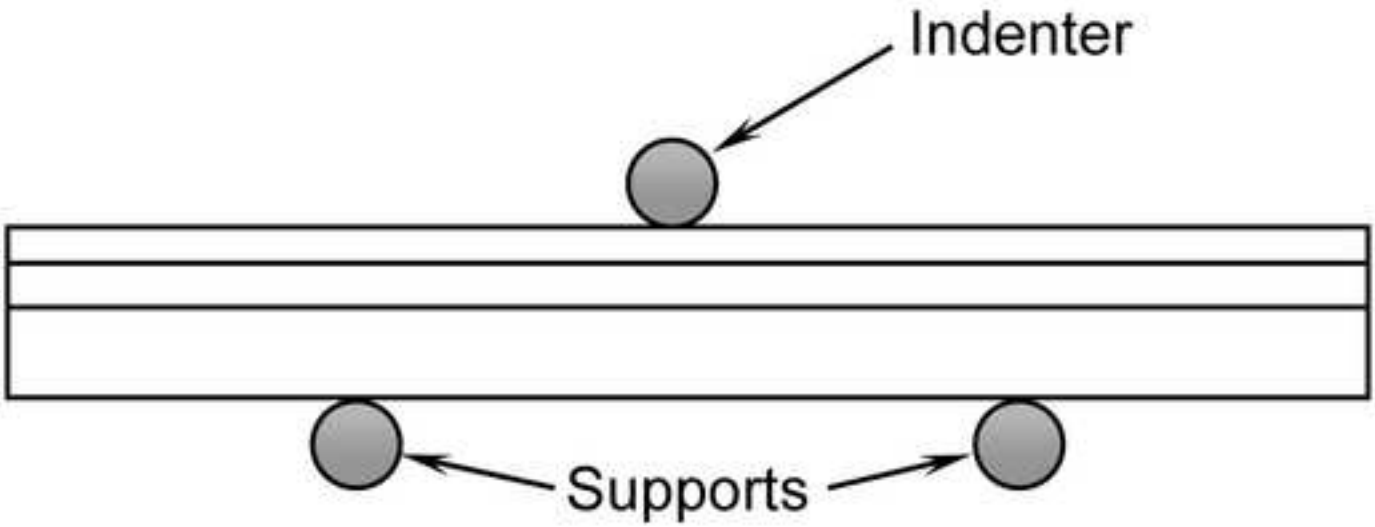

Model B

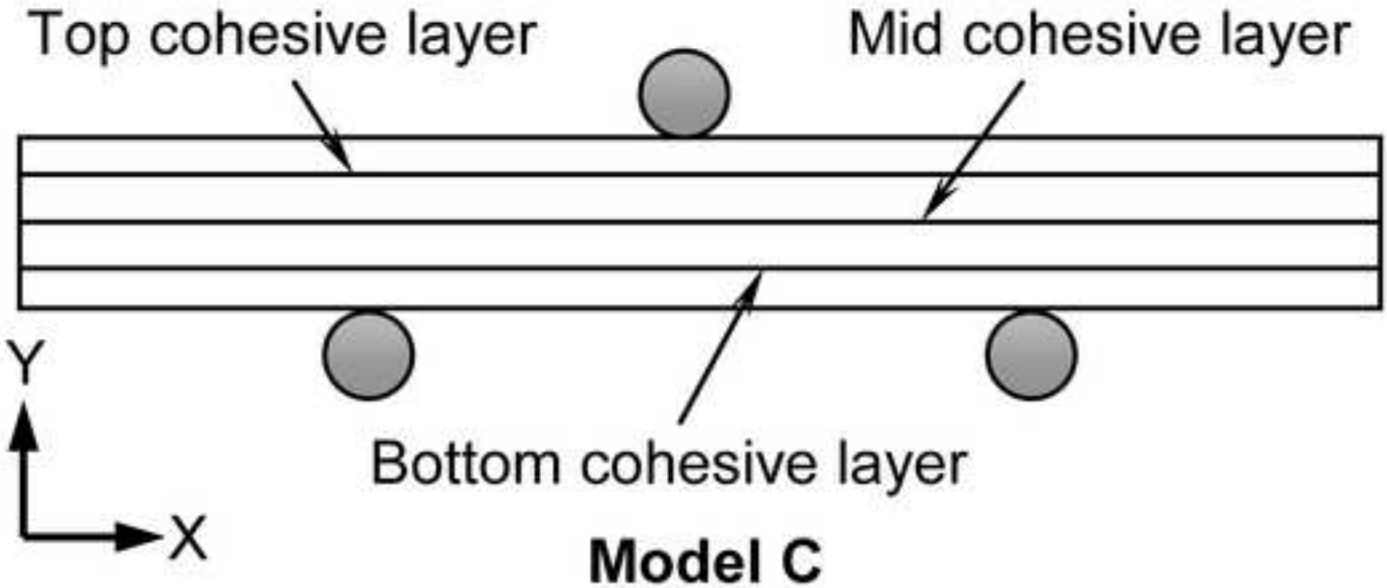

Model C

Figure(s)
Click here to download high resolution image

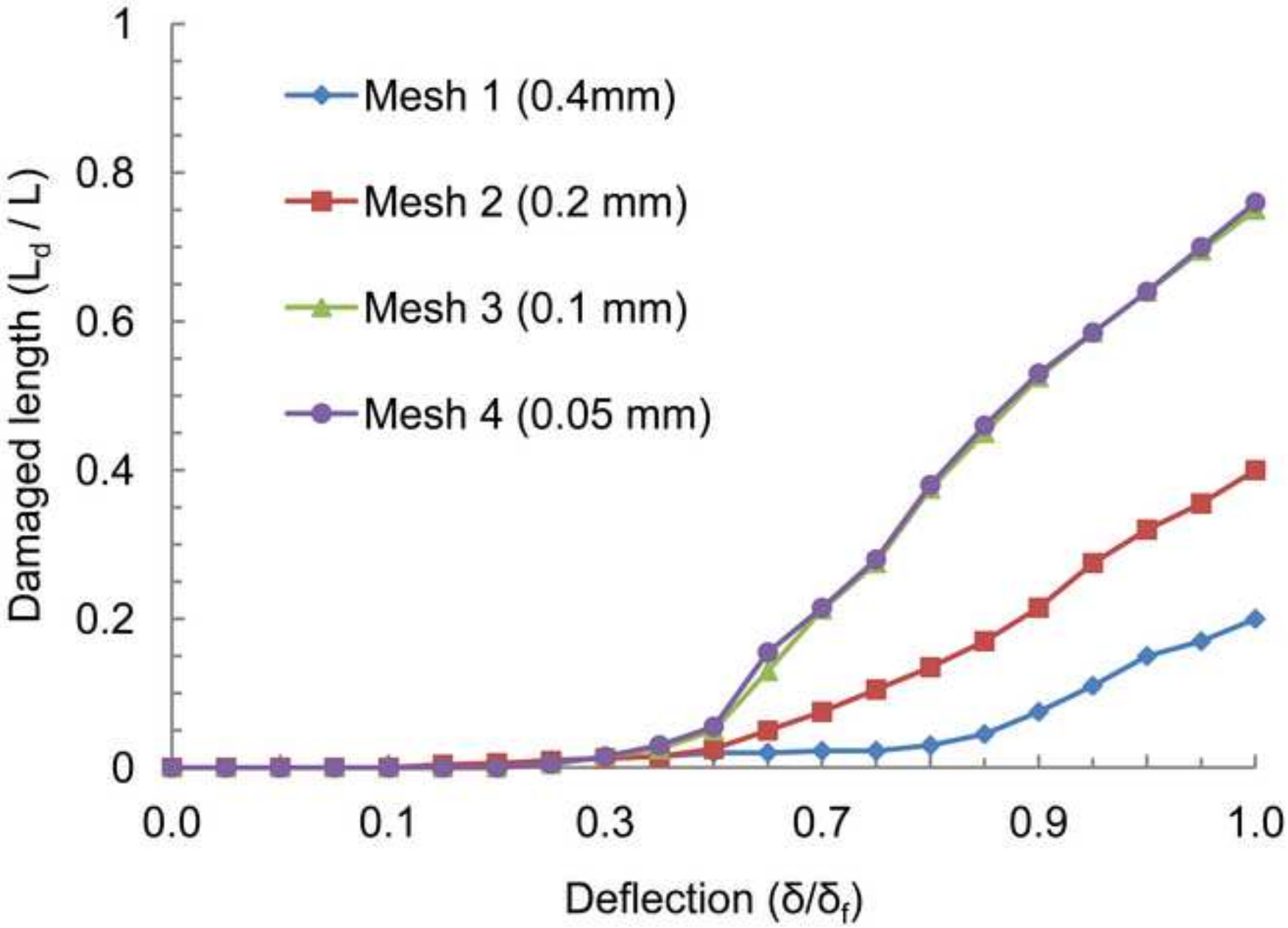

Figure(s)

Click here to download high resolution image

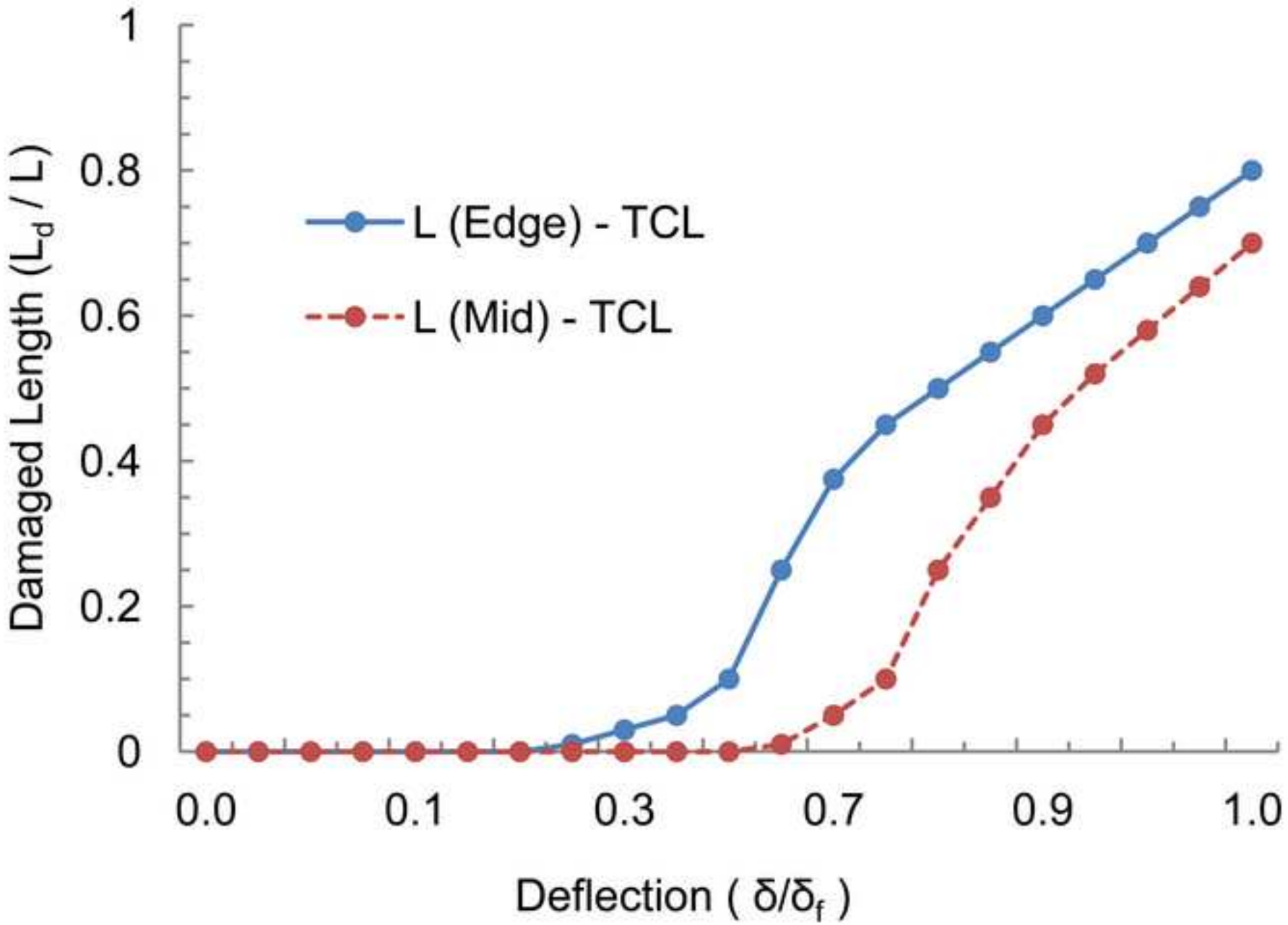

Figure(s)
Click here to download high resolution image

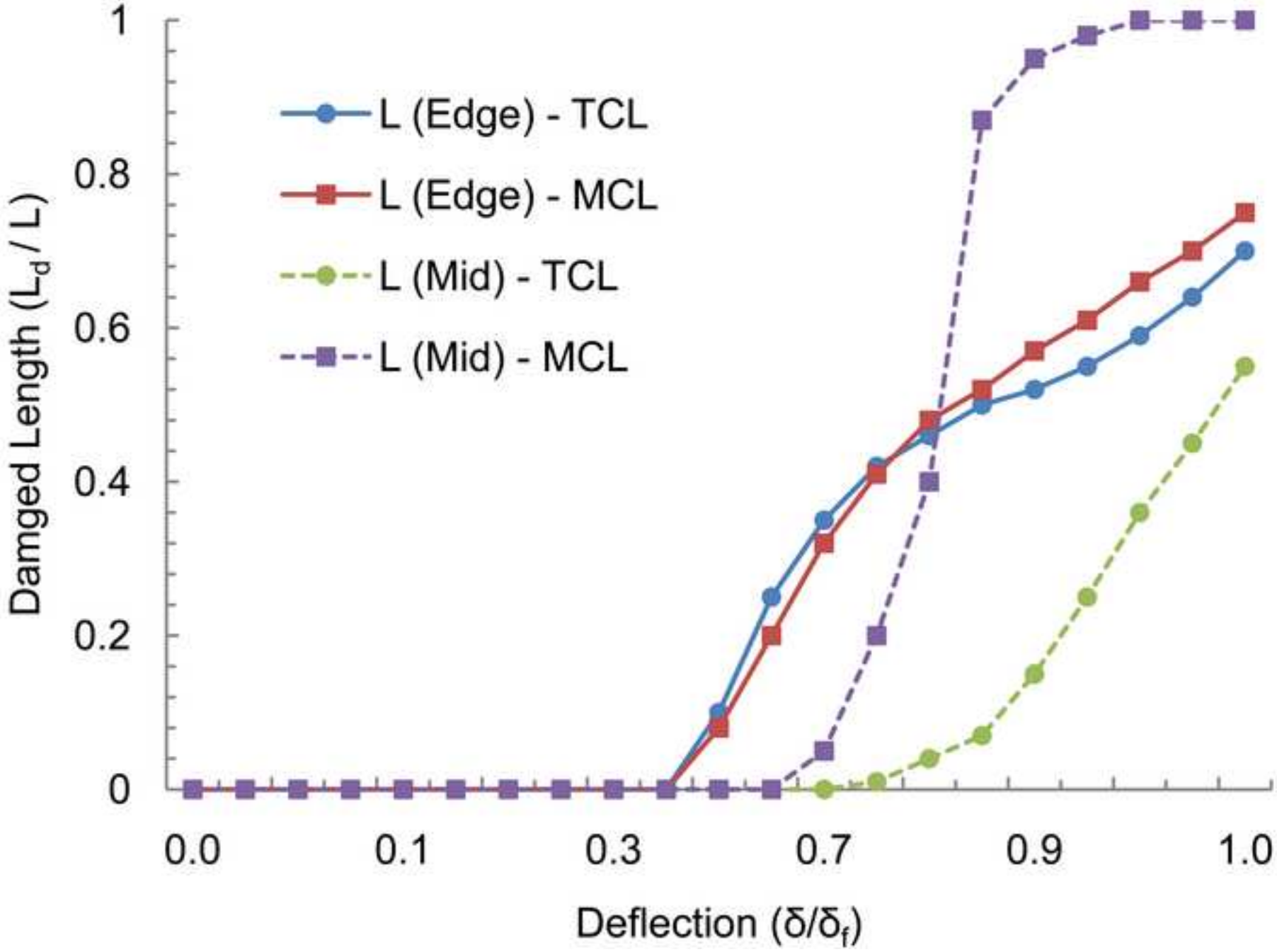

Figure(s)

Click here to download high resolution image

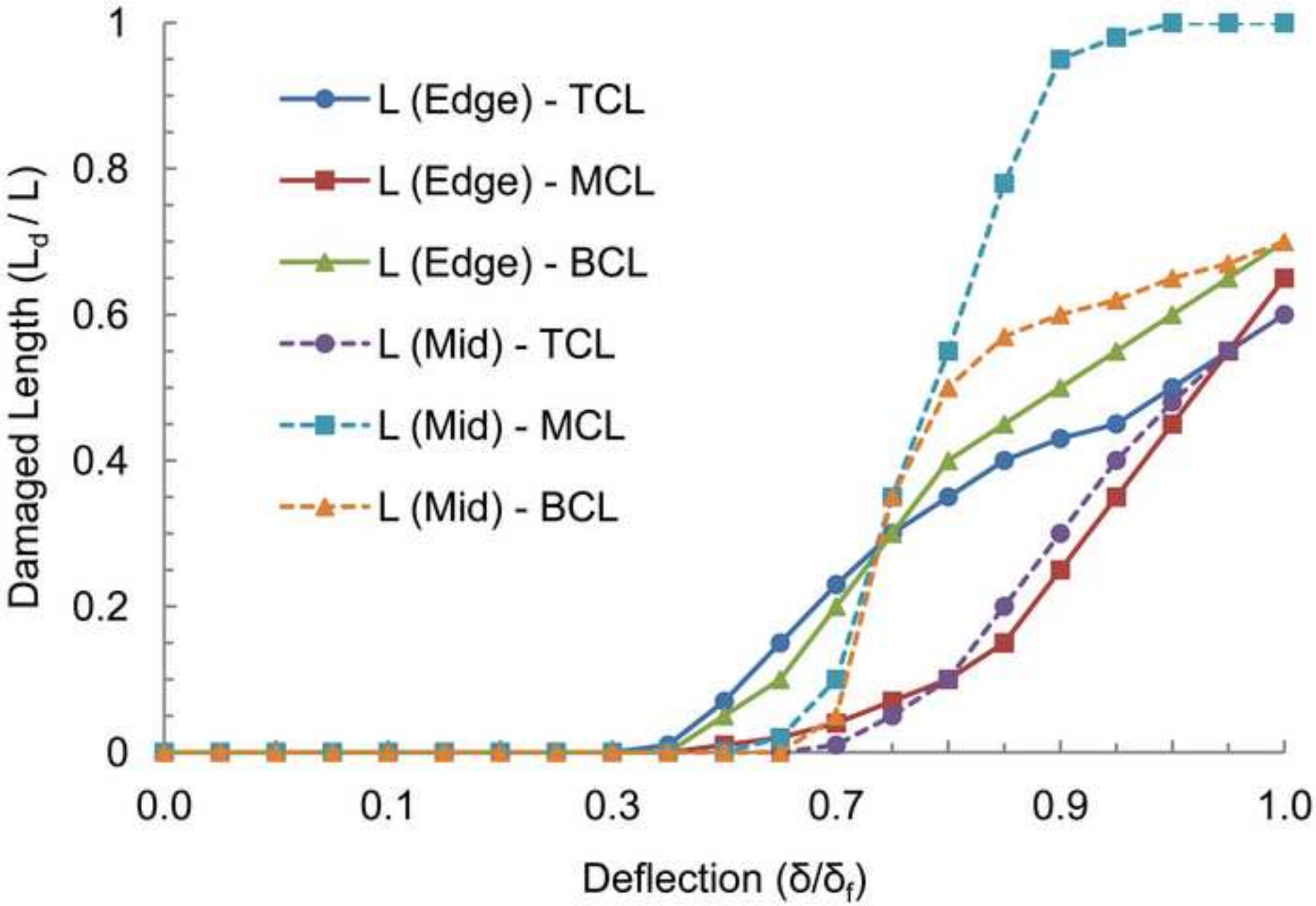

Figure(s)
Click here to download high resolution image

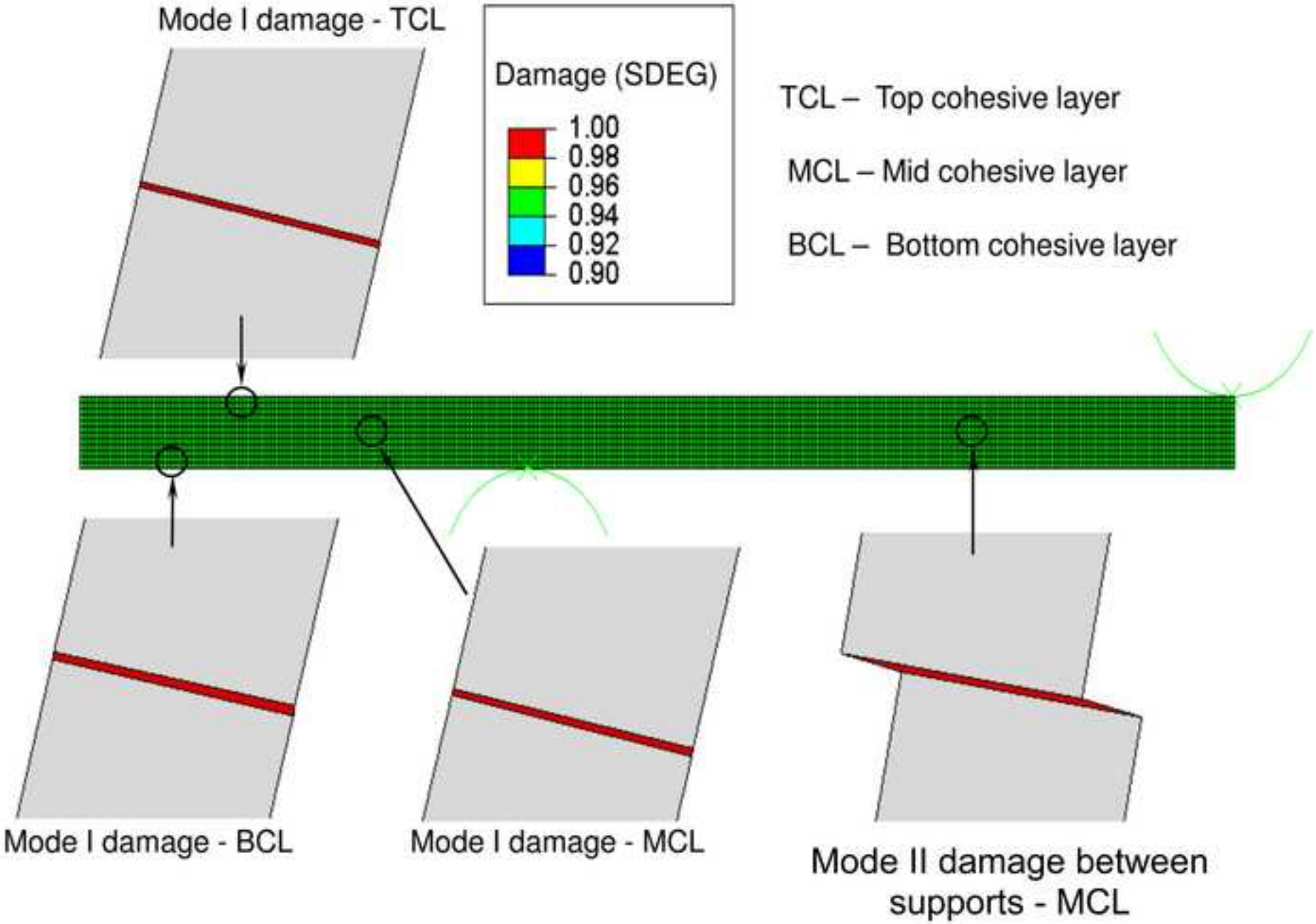

Figure(s)

Click here to download high resolution image

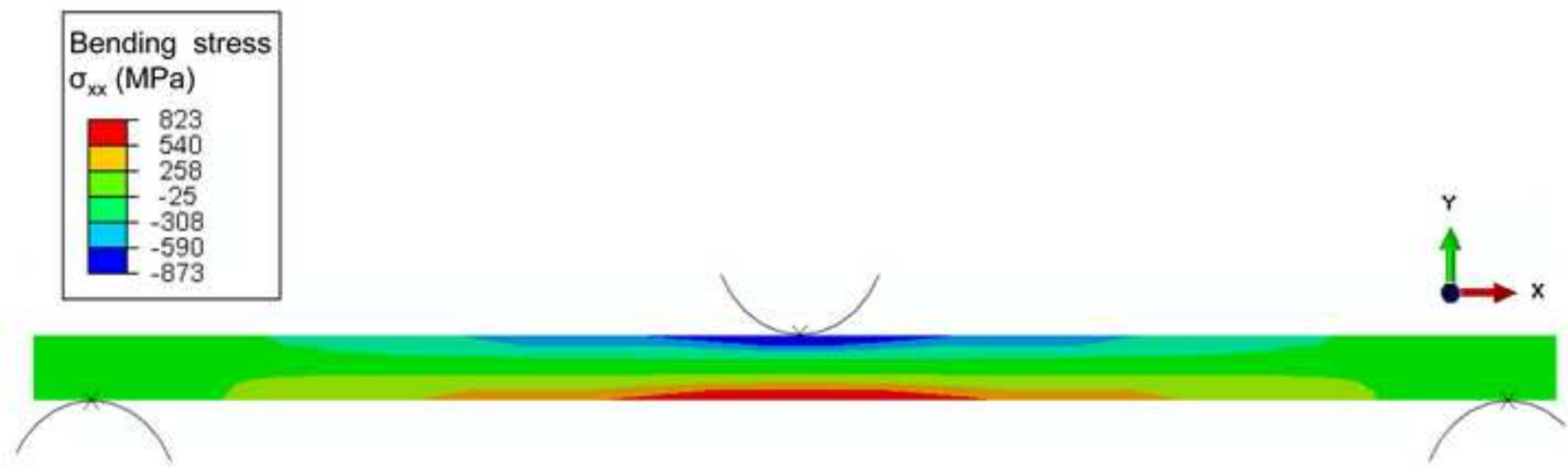

Figure(s)

Click here to download high resolution image

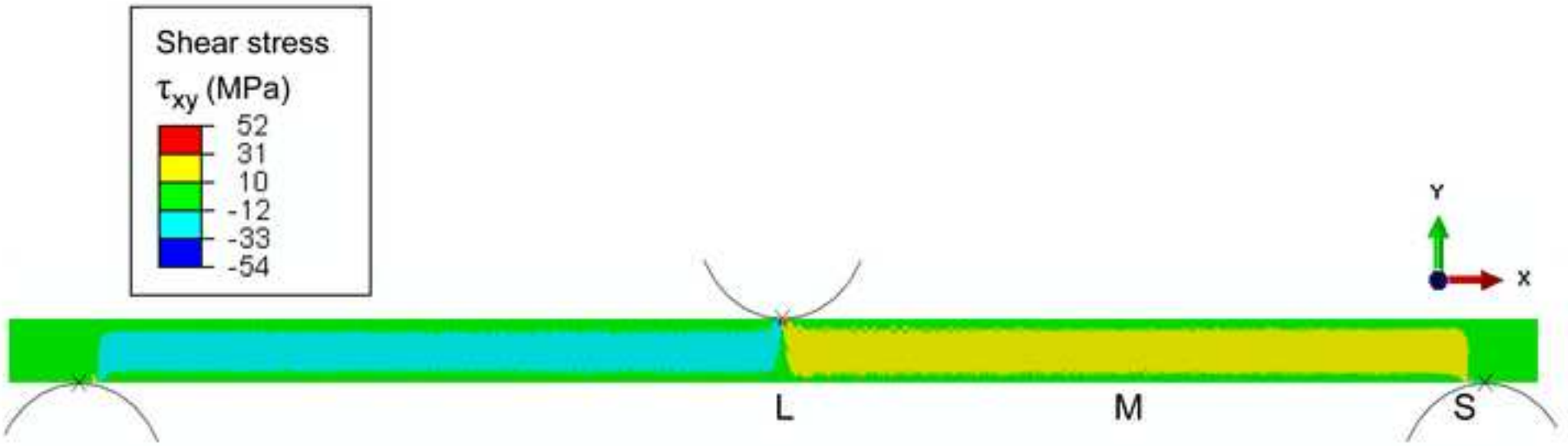

Figure(s)

Click here to download high resolution image

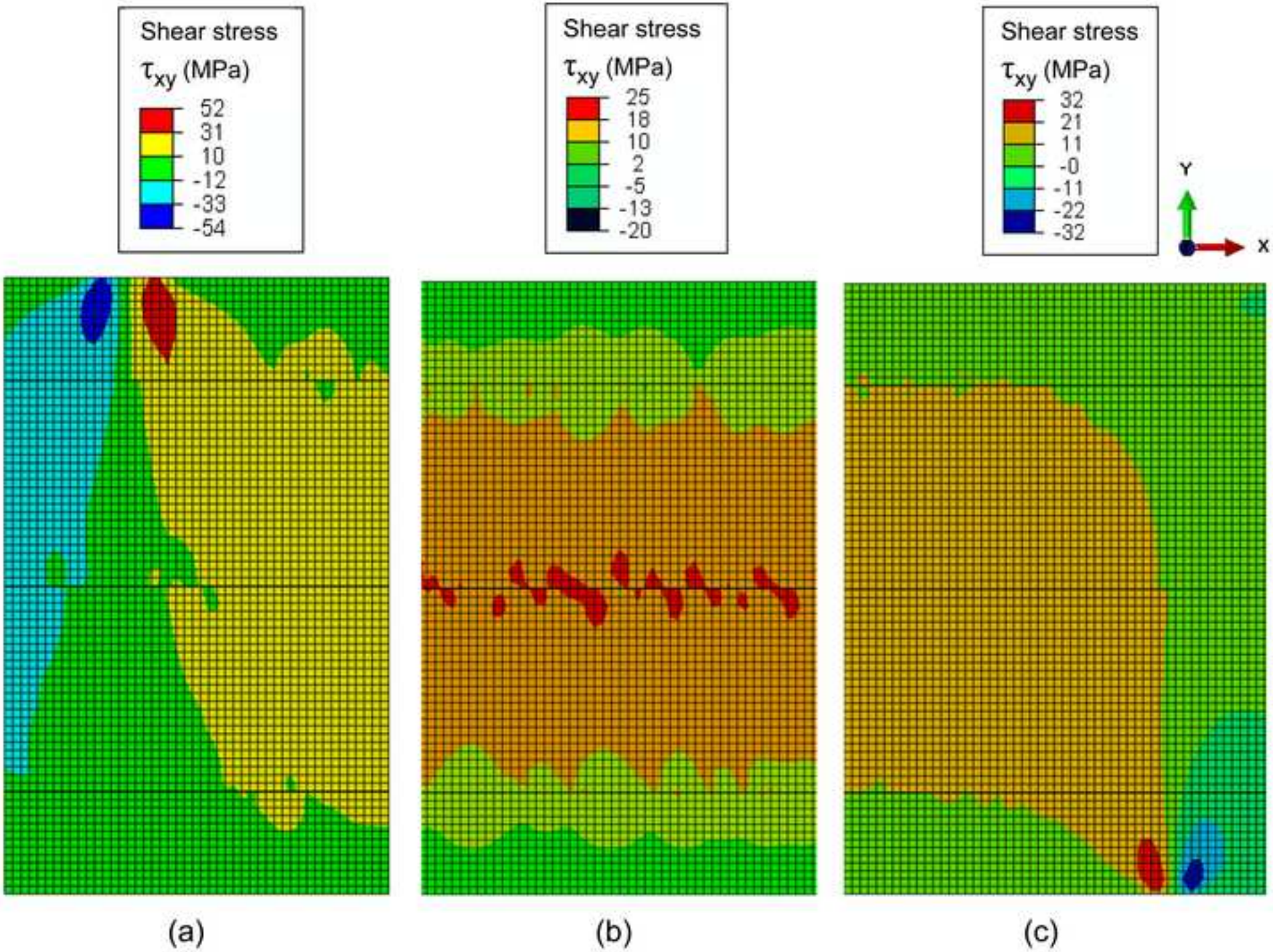

Figure(s)

Click here to download high resolution image

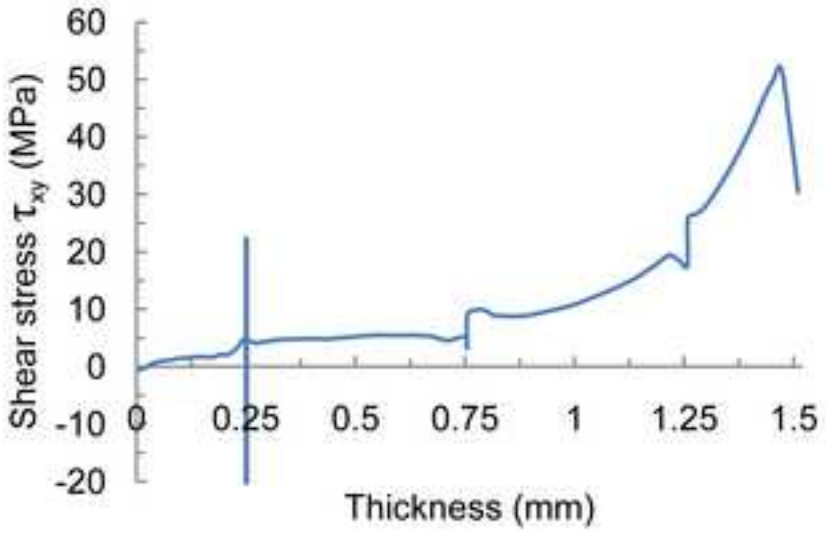

(a)

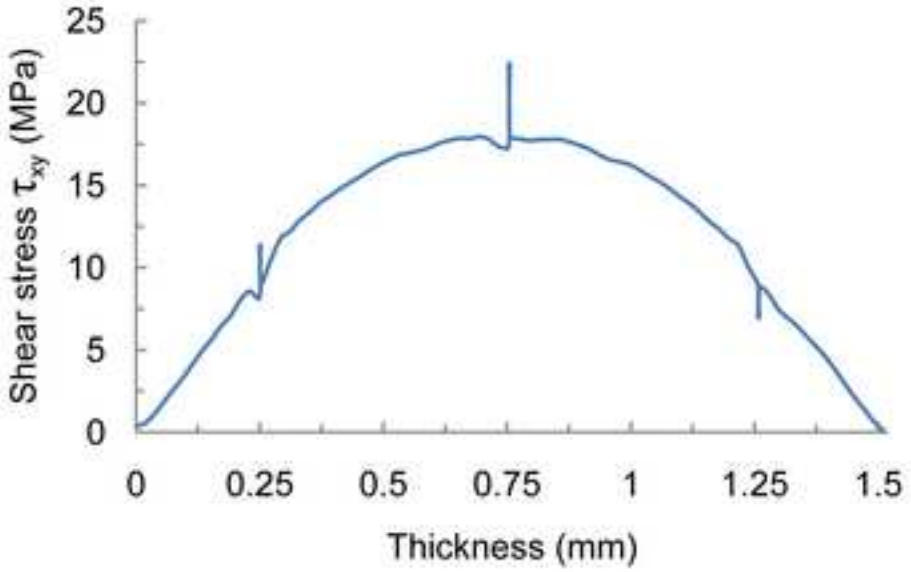

(b)

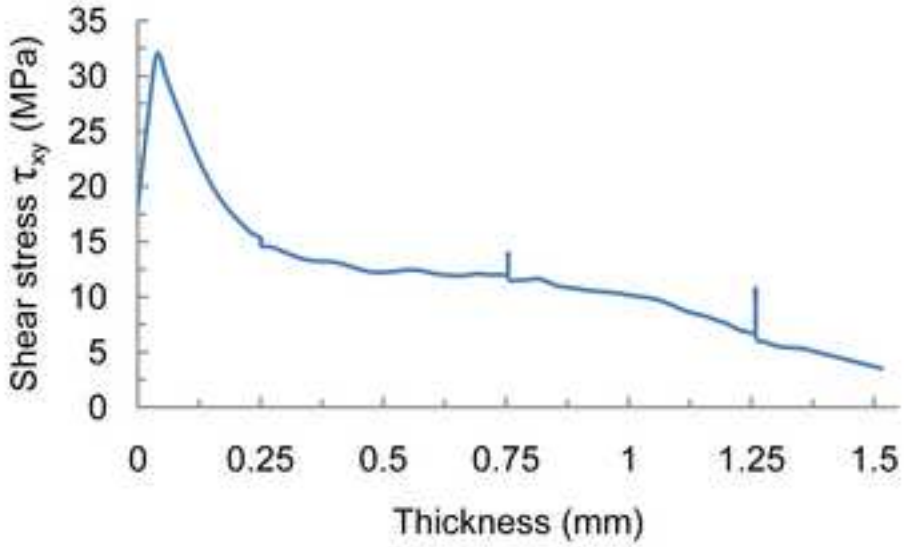

(c)

Figure(s)

Click here to download high resolution image

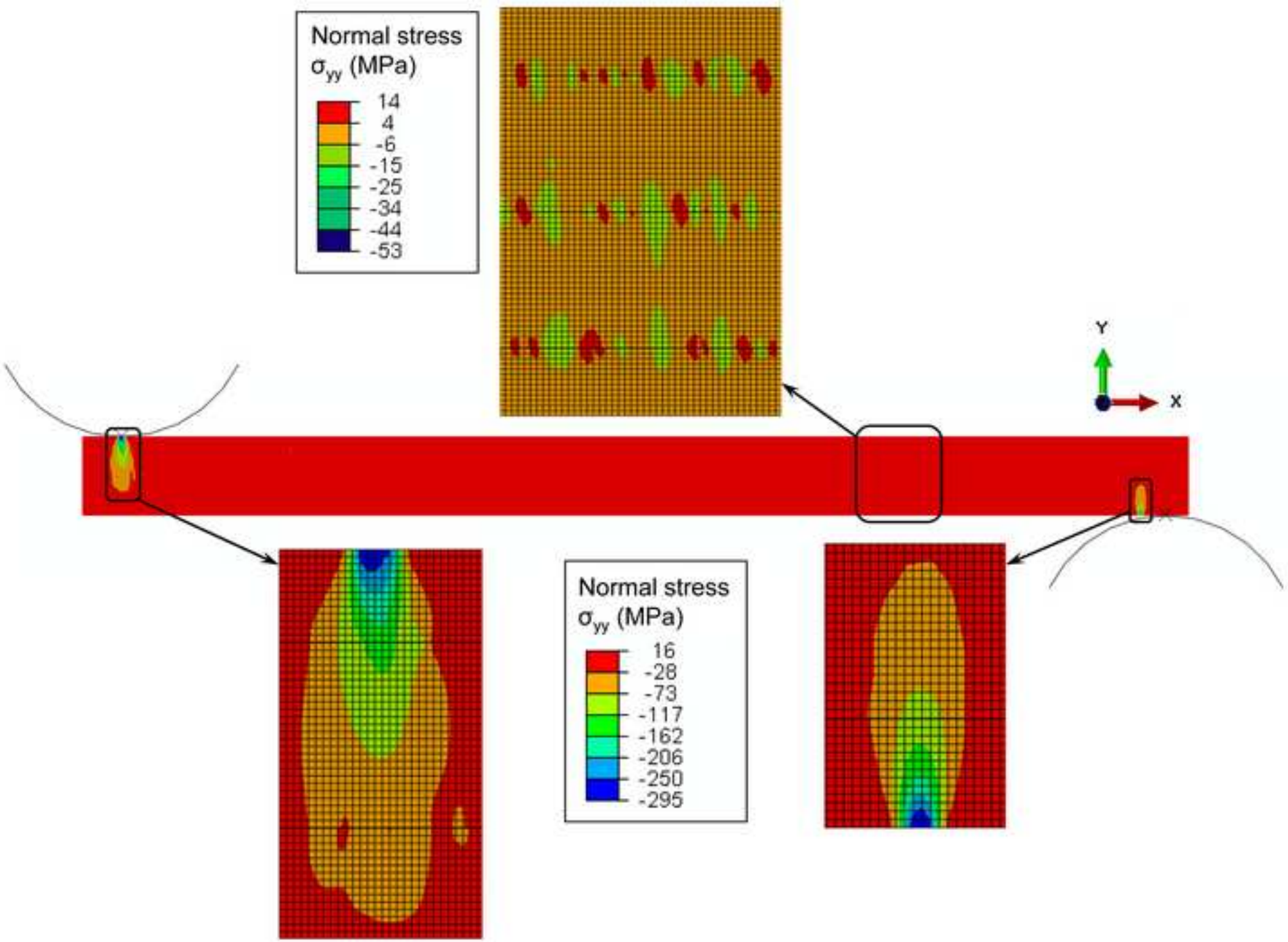

Figure(s)

Click here to download high resolution image

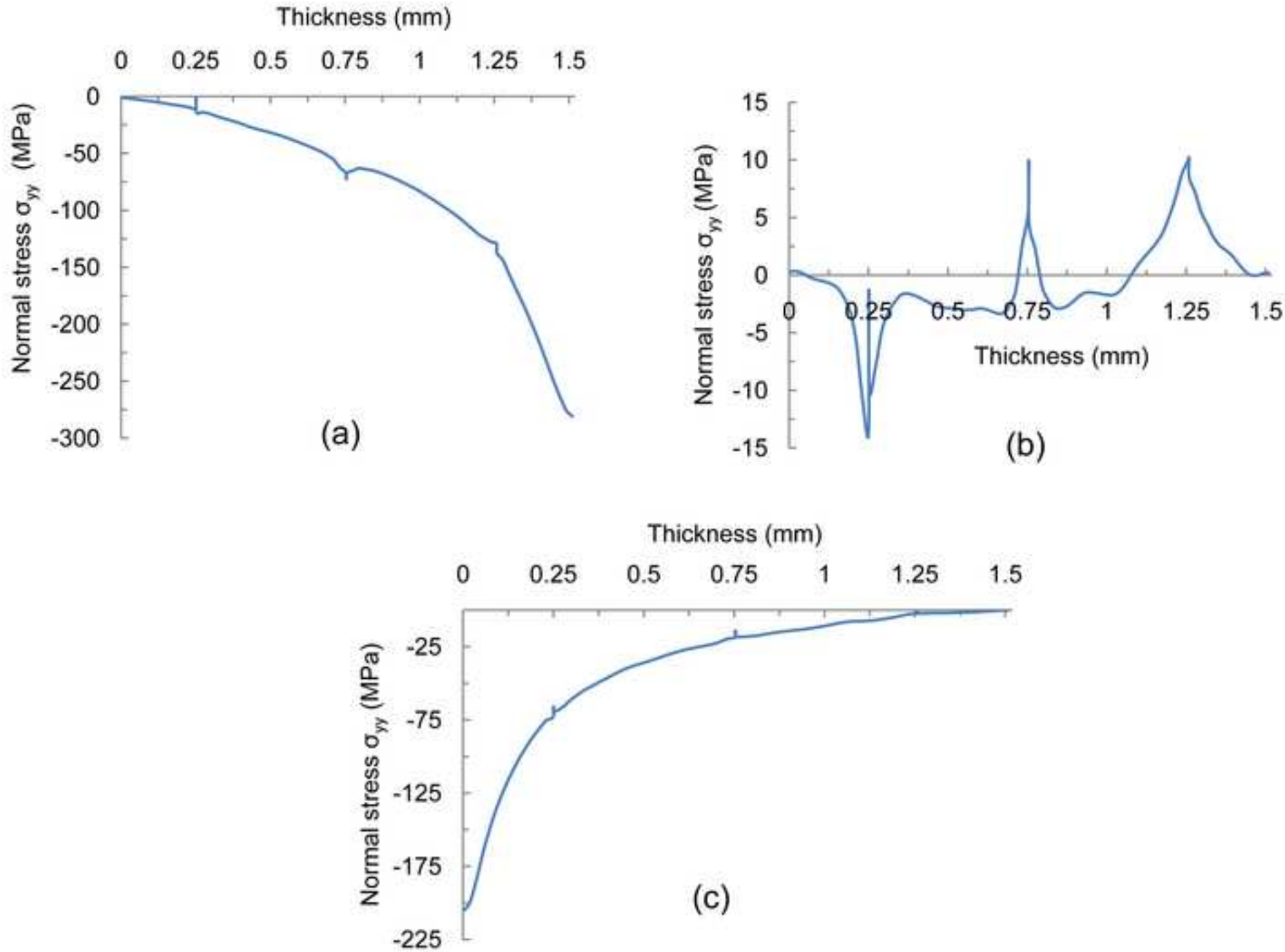

Figure(s)

Click here to download high resolution image